In silico molecular docking and dynamic simulation of antimalarial compounds from Barleria buxifolia root against type III phosphatidylinositol-4-kinase β: Metabolite Profile Analysis Using LC-MS/HRMS

A Abisek
Sri Shanmugha College of Pharmacy
R Poovarasan
Sri Shanmugha College of Pharmacy
T Sathish
Sri Shanmugha College of Pharmacy
G Tamizharasan
Sri Shanmugha College of Pharmacy
Sulekha Khute
University Institute of Pharmacy, Pandit Ravishankar Shukla University
Dr Kareti Srinivasa Rao
Indira Gandhi National Tribal University
Rajesh A
Govt. Siddha Medical College
P. Subash (subash.pharmacy@shanmugha.edu.in)
Sri Shanmugha College of Pharmacy

Research Article

Keywords: Barleria buxifolia, in silico docking, LC-MS/HRMS, malarial target, type III phosphatidylinositol-4-kinase β

Posted Date: January 25th, 2024

DOI: https://doi.org/10.21203/rs.3.rs-3888583/v1

Additional Declarations: No competing interests reported.

Abstract

A member of the Acanthaceae family, *Barleria buxifolia* Linn (*B. buxifolia*) is a shrub of medium size. It originated on the Indian peninsula. Even though the plant is widely used in traditional medicine to treat malaria, no studies have been conducted on this species for antimalarial activity. Box-Behnken design (BBD) modeling was used to optimize the percentage of extraction from the dried root of *B. buxifolia*. The study aims to use high-resolution liquid chromatography-mass spectrometry (LC-MS/HRMS) to discover plant-based components in root extracts of *B. buxifolia*. The observed chromatogram showed the presence of 13 phytoconstituents. For the first time, these phytoconstituents are identified in *B. buxifolia* roots. These phytoconstituents were assessed for their anti-malarial potential against the malaria targets of phosphatidylinositol-4-kinase III β (protein data bank ID: 4D0L, 4WAE) using AutoDock Vina-PyRx software. The anti-malarial potential was compared to known inhibitors of artemisinin and MMV390048. One compound was identified and compared with the standard artemisinin, which showed the best docking score and was further confirmed through in silico SwissADME, admetSAR web server, LigPlot analysis, and MD simulation, i.e., 1-[2-(benzhydryloxy)ethyl]-4-(3-phenylpropyl)piperazine. This *in silico* research plays a crucial role in antimalarial drug discovery, and this research will benefit medicinal chemists by enhancing their understanding and utilization of this phytoconstituents for antimalarial activity.

1. Introduction

Approximately half of the world's population suffers from malaria, a fatal infectious illness that is brought on by five Plasmodium species. Malaria accounts for 77% of pediatric malaria fatalities [1, 2]. Compared to 245 million cases in 2020, there will be 247 million cases in 2021 [3]. The majority of those impacted are the world's poorest, who often turn to traditional remedies due to their accessibility and low cost. The goal of the ethnobotanical study was to document medicinal plants used in malaria prevention and treatment, as well as the preparation and administration techniques, and to gain insight into the diagnosis and understanding of malaria among traditional healers [4, 5].

Bacteria and viruses use phosphoinositide metabolism to ensure efficient replication and survival. Phosphatidylinositol 4-kinase (PI4K) plays a crucial role in virus replication, which is linked to malaria. PI4K-related inhibitors have been found to inhibit virus replication, treat cancer, treat malaria, and reduce organ transplant rejection [6, 7]. MMV390048, a compound used for full chemoprotection in monkeys, has been identified as a molecular target of the Plasmodium parasite PI4K. This compound blocks all life cycle stages of the malaria parasite in a monkey model, which recommends further development and potential contribution to malaria control and eradication [8].

Plasmodium falciparum, the primary malaria parasite, is resistant to standard antimalarial drugs, evading treatment with artemisinin. This resistance necessitates the development of new therapeutics to combat malaria [9]. Quinine and chloroquine poisoning, characterized by severe cardiovascular toxicity, occurs because of the drug’s ability to interfere with the normal electrical conduction of the heart, leading to abnormal heart rhythms. In severe cases, immediate medical intervention is required to stabilize the patient and prevent further complications [10]. Artemisinins have toxic effects on erythropoiesis in both animal and human studies [11]. A report showed that 70–80% of rural communities rely on medicinal plants for primary treatment and traditional and contemporary medicine, with impoverished individuals in developing nations relying on these plants because of their unique nutritional profile [12].

Barleria, a genus of over 300 species in the Acanthaceae family, is known for its diverse taxonomy, cytogenetics, phytochemistry, and pharmacological potential [13]. *Barleria buxifolia* is an attractive shrub with sharp spines and white to pink blooms. Its leaves contain anthelmintic qualities, and it is historically used to cure inflammation, bronchitis, and cough [14]. Barleriaquinone, a root derivative of *B. buxifolia*, was isolated, and its structure was found to be 1-hydroxy-7-methylanthraquinone by decomposition and spectroscopy [15]. Three novel anthraquinones were isolated from *B. buxifolia* roots, and spectrum analysis was used to determine their structures as l-hydroxy-7-carbomethoxy anthraquinone, l-hydroxy-Z-carbomethoxy-7-methylanthraquinone, and l-hydroxy-5-carbomethoxy-7-methylanthraquinone. These newly isolated anthraquinones may show promising potential therapeutic efficacy in various biological activities [16]. A total of 4 Acanthaceae family plants were reported

for antimalarial activity, i.e., *Andrographis paniculata*, *Justicia adhatoda*, *Justicia flava*, and *Acanthus polystachyus* [17–20]. Nonetheless, as far as we are aware, no research on the antimalarial properties of this plant material has been published.

B. buxifolia roots are useful for the treatment of stomach ache, tonic and febrifuge [21], reduce inflammation and cough [22]. Roots and leaves have traditionally been used for cough, bronchitis, and inflammation [23]. A recent study explored the use of the leaf of *B. buxifolia* extract for ultrasonication-enhanced green synthesis of silver nanoparticles, which have the highest antioxidant, antibacterial, and anti-biofilm activity [24]. *B. buxifolia* fraction was isolated using ethyl acetate solvent for antifeedant, larvicidal, and ovicidal activity [25]. GC-MS study of the aerial portions of *B. buxifolia* methanolic extract, a notable ethnomedicinal plant used to cure a variety of diseases [26]. Stem bark, its prophylactic and curative effects on calcium oxalate-induced nephrolithiasis, antimicrobial activity, and the cytotoxic action of two anthraquinones, barleriaquinone-I and barleriaquinone-II, extracted from *B. buxifolia* [27–28]. To the best of our knowledge, this is the first antimalarial study from the root extract of *B. buxifolia.*

A member of the naphthoquinone medication family, atavaquone is used to treat acute, uncomplicated malaria caused by *Plasmodium falciparum* that is resistant to chloroquine in conjunction with proguanil [29]. Recent advancements in promising antimalarial candidates in clinical and preclinical phases, ranging from quinine to the latest marketed drugs [30]. This study has shown that antimalarial compounds were isolated from the root of *B. buxifolia* against PI4KIIIβ using in silico molecular docking and dynamic simulation. Metabolite profile analysis using LC-MS/HRMS. Therefore, the primary goals of this work are as follows: to extract and use LC-MS/HRMS to analyze phytochemicals found in *B. buxifolia* root extract (a); and to utilize *in silico* methods to assess anti-malarial capabilities and find potential lead compounds against the PI4KIIIβ target (b). This study found that it effectively treated the PI4KIIIβ target through *in silico* analysis, confirming previous claims that 1-[2-(benzhydryloxy)ethyl]-4-(3-phenylpropyl)piperazine derivatives were effective in treating trypanothione reductase inhibitors [31]. This study reports for the first time that this compound is effective against the PI4KIIIβ malarial target. Furthermore, this compound's binding energy is higher than that of standard artemisinin, as shown by in silico molecular docking and dynamic simulation.

2. Materials and methods

2.1 Chemicals

The study used analytical-grade solvents such as hydrochloric acid, n-butanol, chloroform, hexane, ammonium hydroxide, acetic acid, and Mayers and Wagner's reagent from Loba Chemie Pvt Ltd.

2.2 Plant collection

In August 2023, fresh *B. buxifolia* roots were collected from the Sankari hills in Salem district, Tamil Nadu. The taxonomist confirmed the identification and classification of the sample with accuracy. This voucher specimen (Ref: 25211) was deposited for reference and can be accessed at the Institute of Forest Genetics and Tree Breeding in Coimbatore, Tamil Nadu, India (Supplementary Fig. 1). Plants were enumerated according to the Natural System of Classification of Bentham and with binomial, local names, descriptions of the plant, and uses.

2.3 Box-Behnken Design

BBD is commonly used (response surface methodology) to efficiently explore the relationship between multiple input variables and a response variable. This design allows the estimation of linear and quadratic effects, making it a versatile tool for optimizing processes and conducting experiments [32]. The three independent variables considered were powder weight, solvent volume, and extraction time and their levels used in BBD (Supplementary Table 1). List of dependent and independent variables in BBD are illustrated in Supplementary Table 2. The single-factor analysis allowed the examination of the unique effects of each independent variable on the dependent variable. This approach provided valuable insights into the unique contributions of each factor to the overall outcome. The inclusion of center points helps to account for any potential bias or variability in the experimental setup, providing a more accurate estimation of the response function. In addition, by calculating pure error, the study can determine the extent to which random factors contribute to the overall variability in the system's performance.

Response surface for the effects of solvent volume and weight of the powder on percentage yield of extraction (Fig. 1). The quadratic equation is given as follows:

$$Y = b0 + b1X1 + b2X2 + b3X3 + b12X1X2 + b13X1X3 + b23X2X3 + b11X12 + b22X22 + b33X32$$

where Y is the dependent variable, b0 is the intercept, and b1 to b33 denote the regression coefficient calculated from the observations of individual responses. X1 through X3 represent the coded levels of prefixed independent variables (X1 is for powder weight, X2 for solvent volume, and X3 is for extraction time). Furthermore, X1 ×2, X1 ×3, X2 ×3, and Xi 2 (i = 1, 2, and 3) are the other factors that indicate the interaction of the independent variable and quadratic terms, respectively. Summary result of regression analysis for variables like Df (degrees of freedom), SS (Sum of squares), Ms (Mean of squares), p-value, F-value, R^2 value, and SD are illustrated in Supplementary Table 3.

2.4 Preprocessing and extraction

The plant roots were dried and ground into a coarse powder using a mechanical grinder. The plant material was macerated in a mixture of 96% ethanol, water, and 37% HCL for three days [33]. The extract was concentrated in a water bath, and the dried extract was partitioned with hexane and methanol. The n-hexane fraction was collected, alkalized with ammonium hydroxide, and chloroform added to the solution.

2.5 Isolation

To separate the chloroform part, it was put through TLC on silica gel G plates (2 × 10 cm) that were mixed with n-butanol, water, and acetic acid [7:2:1]. The TLC plate showed a single spot where the chloroform part had been eluted. The study used column chromatography with silica gel as the stationary phase and a mobile phase/eluent of n-butanol, water, and acetic acid in a 7:2:1 ratio, followed by column separation and gradient elution, and was analyzed using Mayer's and Wagner's tests.

2.6 LC-HR-MS instrumentations

A microliter of an isolated fraction was separated using a SYNAPT-XS HDMS (Model: DBA064). The UPLC Acquity H-Class system was used for the separation of the microliter fraction. The SYNAPT-XS HDMS and UPLC Acquity H-Class system worked together to separate the fraction with high resolution and measure its mass correctly. The following parameters were applied to the liquid chromatographic setup: injection volume of 1 µL, flow rate of 0.3 ml/min, and column temperature of 25°C. 0.1% formic acid in LC-MS-grade acetonitrile solvent (B) and 0.1% formic acid in LC-MS-grade water solvent (A) served as the mobile phase. The mass spectrometer was configured with 10,000 resolution and spectra monitoring in the m/z 50–1500 range. The separation was achieved using a gradient elution, starting with 95% solvent A and 5% solvent B and gradually increasing the proportion of solvent B over time. The total run time was 2 minutes. LC–MS/HRMS chromatogram of extract of *B. buxifolia* root (Fig. 2).

2.7 *In silico* fragmentation and identification of bioactive metabolite mass spectra

The MetFrag architecture is a powerful tool for predicting the fragmentation patterns of metabolites, which can aid in the identification process. The ChEBi database, which works with the MetFrag architecture, has a huge collection of chemical compounds that can be used to accurately match and label bioactive plant metabolites. The ChEBi database and MetFrag architecture were used to identify bioactive plant metabolites. The experimental circumstances of MS acquisition were considered while selecting the method parameters. After selecting the ChEBi candidate database, chemicals were obtained. The fragmentation parameters were set to positive mode, mz ppm, and mzabs. The candidate picture, identifier, precise mass, chemical formula, score, and number are shown in a score-ranked list along with additional facts about each candidate, including structural data, isotopic pattern, and fragmentation pattern. This comprehensive display allowed for a thorough analysis and comparison of the candidates, aiding in the identification of the most likely compound present in the sample [34].

2.8 Experimental

2.8.1 Hardware specifications

This study used an AMD Ryzen 5 5500 U with a Radeon graphics processor running on Windows 11.

2.8.2 Software specifications

The receptor protein structures were retrieved from the PDB database at https://www.rcsb.org. The ligand structures were drawn, and Simplified Molecular Input Line System (SMILES) conversion was performed using ChemDraw 16.0, a trial licensed version from PerkinElmer, Waltham, Massachusetts. The receptor protein structures were analyzed using the AutoDock Vina 1.5.7 available at https://vina.scripps.edu/ and PyRx software for molecular docking studies, downloaded from https://pyrx.sourceforge.io/. Discovery Studio Visualizer V20 for docking verification software is available at https://discover.3ds.com/. The PyMOL software academic license version was downloaded from https://pymol.org/edu/. Drug ability was determined by Lipinski, and GI absorption, synthetic accessibility (SA), and bioavailability were evaluated at http://www.swissadme.ch/. The admetSAR web portal for in silico studies is available at http://lmmd.ecust.edu.cn/admetsar2. LigPlot + V 2.1 for intermolecular analysis using a trial licensed version from https://www.ebi.ac.uk/. The PDB was modeled using the solution builder at https://charmm-gui.org/. Molecular dynamics simulations were performed using NAMD version 2.14, obtained from https://www.ks.uiuc.edu/.

2.9 Preparation of the receptors

The protein data bank (PDB) was used to obtain the structural receptors of PI4KIIIβ (PDB ID: 4D0L and 4WAE). Screening was performed on water molecule heteroatoms and alternative atomic sites separated from protein receptor structures using PyRx 0.8 software [35].

2.10 Preparation of the ligands

The 2D structures of thirteen observed ligands and standard MMV390048 and artemisinin were saved in PDB format. Chem3D was used to reduce energy using the MM2 force field, importing the ligands into the workspace of docking studies [36].

2.11 Molecular Docking Study

Molecular docking is important for identifying the optimal compounds for receptor molecules. Autodock 1.5.7 was used to assess the inhibition ability of compounds against hypothetical protein structures, and energy was minimized using a universal force field and conjugate gradient algorithm. Proteins and ligands were converted into the PDBQT format. PyRx is a virtual screening tool for computer-aided drug design that enhances docking protocols. It sets coordinates for the Vina search space center consecutively at about 4D0L (X: 8.1918 x Y: 335.387 x Z: 51.2460). Å and number of points was designed as 262 × 275 × 324 for the X, Y, and Z axis and 4WAE (X: 18.7237 x Y: 39.3369 x Z: -10.4817). Å and number of points were designed as 53 × 45 × 50 for the X, Y, and Z axis, respectively. Top docked ligands and standard drugs with protein complex binding positions were inspected using the Biovia Discovery Studio 2021 Client [37].

2.12 *In silico* analysis

SwissADME and admetSAR data sources require the use of SMILES to represent a compound's chemical structure. This notation facilitates drug development by enabling the calculation of physicochemical descriptors and forecasting small-molecule pharmacokinetics and drug-likeness [38]. The SwissADME web portal provides information on Lipinski, gastrointestinal (GI) absorption, synthetic accessibility, and bioavailability [39]. The admet-SAR web portal provides information on acute oral toxicity, plasma protein binding, water solubility, and carcinogens [40].

2.13 LigPlot analysis

A useful tool for investigating and visualizing the interactions between ligand and protein complexes is LigPlot, which provides comprehensive details on the binding method of ligands, intermolecular interactions, and atom spatial arrangement. To facilitate the creation of novel medicinal compounds, LigPlot identifies the shared binding site between the lead-hit ligand and conventional medication. Additionally, LigPlot allows researchers to compare multiple ligand-protein complexes, enabling them to identify similarities and differences in binding patterns across different compounds. LigPlot is a program that creates a ligand interaction plot, providing crucial insights into the binding mechanism and affinity of ligands to proteins, including hydrogen bonds, hydrophobic interactions, and electrostatic interactions, for improved ligand design. These visual representations can

help researchers visualize and analyze the specific molecular interactions that contribute to the binding affinity and stability of the ligand-protein complex. Overall, LigPlot serves as a valuable tool for drug discovery and optimization by providing detailed information on ligand-protein interactions. Additionally, LigPlot can be used to compare multiple ligand-protein complexes, aiding in the identification of common binding motifs or structural features that may be important for ligand recognition and binding [41].

2.14 Molecular dynamics simulation

The stability of protein-ligand complex lead and protein-standard MMV390048 was assessed using MD simulation using the Nanomolecular Dynamics (NAMD) program [42]. The CHARMM-GUI online service generated ligand topology files [43, 44]. MD simulations were conducted at 310 K for 50 ns to investigate stability, improve docking results, and understand enzyme-target interactions in the docked ligand-target complex. A high-throughput dynamic simulation process was established to examine the ligand-target receptor binding mechanism under specific circumstances.

3. Results

3.1 Design of the experiment

Powder weight, solvent volume, and extraction time were among the variables taken into account for optimizing the extraction yield using a Box-Behnken design. To identify the key extraction process components, a two-level fractional factorial design was used. The experimental design coded each independent variable at three different levels (-1, 0, and + 1) as illustrated in Supplementary Table 1. The powder weight (25–75 g), solvent volume (150–450 ml), and extraction time (24–72 hrs) were varied in three levels, based on the equipment's limits and mild temperatures. Design experiments and analyses were conducted using Design Expert 12 software, ensuring accurate results. Supplementary Table 2 represents the extraction conditions and yields of the BBD extracts. High powder content yields and reduced selectivity significantly increase the yield. Differences in yield were observed at 0.9% (w/w) for the best extraction. The only significant parameter affecting the extraction yield is the response surface methodology. The response surface methodology graphics are shown in Fig. 1.

3.2. Putative identification bioactive compound in *B. buxifolia* by LC-MS/HRMS

Qualitative analysis of the *B. buxifolia* fraction by LC-MS/HRMS revealed the presence of 13 compounds (Supplementary Table 4).

3.3 Identification of new compounds from *B. buxifolia*

The reported phytoconstituents from the *B. buxifolia* root extract were compared with the phytoconstituents presently identified by LC-MS/HRMS [15, 16]. These thirteen phytoconstituents were identified for the first time in the root material of *B. buxifolia*.

3.4 Ligand preparation

LC-MS/HRMS-identified phytoconstituents from *B. buxifolia* and standard known inhibitors of malaria (MM390048 and artemisinin) were considered ligands (Supplementary Fig. 2).

3.5 Molecular Docking Study

This study predicts the best-pose compounds for their interactions with malarial targets of PI4KIIIβ. Potential lead compounds were identified on the basis of their least binding energy (high docking score) with the receptors. AutoDock Vina-PyRx docking studies confirm that phytoconstituents from *B. buxifolia* root extract have the best binding affinity to malarial targets. Table 1 shows the binding energy between the LC-MS/HRMS-identified ligand interactions with the selected PI4KIIIβ receptors.

Table 1
Docking score of phytoconstituents from the root extract of *B. buxifolia*

Ligand No	Compound Name	Binding energy (Kcal/mol)	
		4D0L	4WAE
1	(3R)-3-Hydroxy-D-aspartate(1-)	-4.6	-6.4
2	(2,3-bis(ethylthio)-6-methoxy-1*H*-inden-ol)	-5.9	-6.4
3	6-cis-Docosenamide	-4.9	-5.4
4	Plakortolide P	-6.5	-6.6
5	Metachromin S	-7.1	-8.1
6	1-[2-(Benzhydryloxy)ethyl]-4-(3-phenylpropyl)piperazine	-8.8*	-8.6*
7	N-Palmitoylhexadecasphinganine	-5.3	-5.8
8	N-Tetradecanoylicosasphinganine	-5.0	-6.3
9	2,3-Bis-O-(geranylgeranyl)-sn-glycero-3-phospho-L-serine(1-)	-7.0	-7.5
10	1-(7Z-hexadecenoyl)-2-(4Z,7Z,10Z,13Z,16Z,19Z-docosahexaenoyl)-sn-glycero-3-phosphocholine	-5.8	-6.3
11	Oligomycin B	-9.7*	-9.4*
12	DilC18(3) dye	-4.5	-4.6
13	Beta-sitosterol glucoside-3"-O-hexacosanoicate	-7.9	-6.3
Std1	MMV390048	-9.1	-8.6
Std2	Artemisinin	-8.1	-7.8

3.6 Top dock score phytoconstituent interaction with 4D0L

Two compounds had a higher docking score than the standard drug, such as oligomycin B (-9.7) and 1-[2-(benzhydryloxy)ethyl]-4-(3-phenylpropyl)piperazine (-8.8).

3.7 Top dock score phytoconstituent interaction with 4WAE

Two compounds were shown to have a higher docking score than the standard drug, such as oligomycin B (-9.4) and 1-[2-(benzhydryloxy)ethyl]-4-(3-phenylpropyl)piperazine (-8.6).

3.8 Prediction of binding sites

The docking chain view and interaction profiles of PI4KIIIβ targets with the lead phytoconstituent, i.e., 1-[2-(benzhydryloxy)ethyl]-4-(3-phenylpropyl)piperazine, and the standard inhibitors MMV390048 and artemisinin (Figs. 3 and 4). The examination of docking findings was validated using Discovery Studio Visualizer to assess the interaction sites.

3.9 *In silico* analysis

Based on the docking score, the most promising two ligands and standards were analyzed through the Swiss ADME and AdmetSAR, as illustrated in Table 2. One ligand specifically failed in Lipinski and GI absorption, i.e., oligomycin B. Moreover, phase 1 clinical trial standard MMV390048 has low GI absorption and low plasma protein binding. The remaining ligand (1-[2-(benzhydryloxy)ethyl]-4-(3-phenylpropyl)piperazine) and standard artemisinin met the criteria of the pharmacokinetic properties like Lipinski rule, high gastro-intestinal absorption, synthetic accessibility, better bioavailability, acute oral toxicity, plasma protein binding, water solubility, and no carcinogen effect.

Table 2
SwissADME and admetSAR property of the selected top ligands and standards

Ligand No	Protein(s)	SwissADME				admetSAR			
		Lipinski	GI absorption	Synthetic accessibility	Bioavailability score	Acute Oral toxicity (mol/kg)	PPB	WS (logS)	Carcinogen (binary)
11	4D0L, 4WAE	No	Low	10.00	0.17	2.625	0.747	-3.466	Negative
6*	4D0L, 4WAE	Yes	High	3.12	0.55	2.207	1.161	-1.918	Negative
Std1	4D0L, 4WAE	Yes	Low	2.89	0.55	2.222	0.94	-3.612	Negative
Std2*	4D0L, 4WAE	Yes	High	3.16	0.55	2.169	1.039	-3.222	Negative

GI absorption: Gastrointestinal absorption, PPB: Plasma Protein Binding; WS: Water solubility

3.10 LigPlot analysis

The target protein complex with the lead hit (1-[2-(benzhydryloxy)ethyl]-4-(3-phenylpropyl)piperazine) and standard artemisinin were analyzed using LigPlot software. The compounds with favorable intermolecular interactions were observed under LigPlot analysis to examine their H-bond interactions and hydrophobic contacts. The resulting comparisons with the artemisinin standard are shown in Table 3 and Fig. 5. The 4D0L complex with 1-[2-(benzhydryloxy)ethyl]-4-(3-phenylpropyl)piperazine showed 16 hydrophobic contacts; the 4D0L complex with standard artemisinin showed 11 hydrophobic contacts; and one H-bond interaction was observed. Seven common binding sites were observed between lead-hit and standard artemisinin, i.e., Ala692 (A), Met777 (A), Ser781 (A), Gly780 (A), Tyr650 (A), Glu162 (F), and Phe693 (A). Similarly, the 4WAE complex with 1-[2-(benzhydryloxy)ethyl]-4-(3-phenylpropyl)piperazine showed 14 hydrophobic interactions, and the 4WAE complex with standard artemisinin showed 10 hydrophobic contacts. Six common binding sites were observed between lead hit and standard artemisinin, i.e., Phe174 (A), Asp173 (A), Pro177 (A), Leu573 (A), phe576 (A), and Gln211 (A).

Table 3
Protein-ligand interaction analysis using LigPlot software

Complex	H-bond interactions		Hydrophobic contacts
	Amino acid	Distance (Å)	Amino acid
4D0L-ligand 6	-	-	Cys646(A), Tyr650(A), Glu759(A), Arg760(A), Ala692(A), Phe693(A), Met777(A), Gly780(A), Arg30(F), Phe31(F), Asn34(F), Vall61(F), Ser158(F), Glu162(F), His762(A), Ser781(A).
4D0L-Std 2	Phe693(A)	3.19 Å	Tyr650(A), Ala692(A), Leu773(A), Gln776(A), Met777(A), Gly780(A), Ser781(A), Asn160(F), Glu162(F), Ala163(F).
4WAE-ligand 6	-	-	Glu170(A), Asp173(A), Pro177(A), Phel74(A), Gln211(A), Pro370(A), Leu573(A), Phe576(A), Lys580(A), Gln581(A), Ser584(A), Lys599(A), Ile600(A), Leu601(A).
4WAE – Std 2	-	-	Asp173(A), Phe174(A), Leu176(A), Pro177(A), Ser205(A), Asn207(A), Phe208(A), Gln211(A), Leu573(A), Phe576(A).

3.11 Molecular dynamics (MD) simulation

The shortlisted ligand 1-[2-(benzhydryloxy)ethyl]-4-(3-phenylpropyl)piperazine and standard artemisinin were used to study protein-ligand complexes using MD simulation. The structural aberrations in the protein (4D0L and 4WAE) and its docked complexes were assessed by analyzing the systematic features of each complex, such as RMSD and RMSF, for 50 ns. To monitor conformational and structural changes in the backbone atoms of protein-ligand complexes, RMSD and RMSF analyses

(Figs. 6 and 7) were performed, and the results are illustrated in Table 4. The RMSD and RMSF plots of protein-ligand complexes were calculated for all complexes for a 50-ns trajectory. The research assessed the stability and movement of protein-ligand complexes and ligand-associated molecules in a hydrated environment to evaluate their structural stability.

Table 4
The average values of RMSD and RMSF of lead hit from *B. buxifolia* and standard artemisinin.

S. No	Complex	Average ± SD RMSD (nm)	Average ± SD RMSF (nm)
1.	4D0L-ligand 6	0.499 ± 0.080	0.249 ± 0.087
2.	4D0L-std artemisinin	2.282 ± 1.257	1.295 ± 0.588
3.	4WAE-ligand 6	0.426 ± 0.054	0.178 ± 0.105
4.	4WAE –Std artemisinin	1.016 ± 0.102	0.259 ± 0.177

3.11.1 RMSD

In biological systems, these motions are essential for efficiency and dependability of operation. As seen in Fig. 6, the system as a whole showed notable stability. Over the 50-ns simulation period, the RMSD of the bound protein-ligand combination remained constant. 4-[2-(benzhydryloxy)ethyl]-4-(3-phenylpropyl)piperazine had an average RMSD value of 0.499 Å, peaking at 0.63 Å at 40.20 ns. At 39.95 ns, the greatest RMSD value of 3.14 Å was recorded for 4D0L containing artemisinin, with an average value of 2.282. 4-[2-(benzhydryloxy)ethyl]-4-(3-phenylpropyl)piperazine had an average RMSD value of 0.499 Å, with a peak range of 0.51 Å at 48.00 ns. At 29.35 ns, the greatest RMSD value of 1.11 Å was reached for 4WAE with artemisinin, an average of 1.016 Å. The stability of the protein structure and the intensity of ligand attachment inside the active site pocket are shown by the RMSD spectrum, which did not reveal any large structural alterations.

3.11.2 RMSF

For every residue in the corresponding system, the RMSF parameter gives important information on the structural flexibility of 4D0L and 4WAE. Based on Fig. 7a, the average fluctuations of 4D0L containing 1-[2-(benzhydryloxy)ethyl]-4-(3-phenylpropyl)piperazine and 4D0L containing artemisinin were 0.249 and 1.295 nm in the present system. Similar to this, Fig. 7b illustrates the average fluctuations of 4WAE with 1-[2-(benzhydryloxy)ethyl]-4-(3-phenylpropyl)piperazine and 4WAE with artemisinin, which were 0.178 and 0.259 nm.

4. Discussion

Traditional optimization techniques like "one factor at a time" can be time-consuming and lead to misleading results due to a lack of interactions between factors. Response surface methodology, such as the Box-Behnken design, optimizes multiple variables and predicts optimal conditions with minimal experimentation. This method allows calculations at intermediate levels that have not been experimentally studied, allowing for more accurate results. The three-stage Box-Behnken design was used in this study, allowing for minimal experimentation in determining optimal conditions [47].

The powdered root of *B. buxifolia* was extracted using maceration and isolated phytoconstituents from crude extract. Metabolites are challenging to detect using MS data because of their diverse physical and chemical makeups. Currently, mass-based search is the primary method used for metabolite identification in untargeted metabolomics studies, with manual verification following. A chemical ion of interest's m/z value is first compared to the database(s). The computational metabolomics community is enhancing methods for identifying known and unknown metabolites. The methods employ two primary strategies: in silico prediction of fragmentation MS/MS spectra from known compounds and in silico prediction of molecular substructures and general chemical properties of unknowns [48]. Machine learning approaches have significantly improved metabolite identification and structural identification, with ChEBI enrichment analysis and MetFrag being useful tools for metabolite identification and computer-assisted metabolite mass spectra identification [49]. Many studies may produce

molecules not annotated to ontology classes, so molecules in ChEBI serve as a sample of the complete set provided by the study or pipeline [50]. A total of 13 phytoconstituents were identified in *B. buxifolia* root extract using LC-MS/HRMS (Supplementary Table 4). These phytoconstituents were the first-time detection of *B. buxifolia* root phytoconstituents.

Phosphatidylinositol 4-kinase (PI4K) is a lipid kinase found in all eukaryotic species responsible for producing phosphatidylinositol 4-phosphate (PI4P), a member of the phosphoinositide family [51]. PI4Ks are divided into two groups, type II and type III, with α and β isoforms in each [52]. For the treatment of malaria, PI4KIIIβ is a possible therapeutic target. It is essential for controlling cellular activity and synthesizing membrane polyphosphoinositides [53]. An essential component of the malaria parasite's survival in both the host and vector is the protease kinase enzyme PfPI4KIIIβ [54].

It has been found that three common anti-Plasmodium chemical classes-artemisinin and MMV390048 inhibit Plasmodium's multistage development [55, 56, 57]. A Phase 1 clinical study including MMV390048, a member of the 2-aminopyridine family, demonstrated the antimalarial action of the plasmodium PI4K inhibitor [58, 59]. These phytoconstituents were examined in further detail as PI4KIIIβ malarial targets (4D0L, 4WAE). Thirteen phytoconstituents were screened using molecular docking against the PI4KIIIβ protein, and two lead compounds with a greater binding potential than standard compounds were found against two selected targets, i.e., 1-[2-(benzhydryloxy)ethyl]-4-(3-phenylpropyl)piperazine and oligomycin B. Moreover, these best dock ligands and standards were screened through the SwissADME and admetSAR properties. Oligomycin failed the criteria of Lipinski and GI absorption. Similarly, the standard MMV390048 drug also failed in GI absorption and plasma protein binding (PPB). At 4D0L and 4WAE, both targets for lead-hit phytoconstituents showed through in silico analysis like Lipinski, GI absorption, synthetic accessibility, bioavailability, acute oral toxicity, PPB, water solubility, and no carcinogen effect, i.e., 1-[2-(benzhydryloxy)ethyl]-4-(3-phenylpropyl)piperazine. This compound and standard artemisinin were further tested for MD simulation, which showed better stability and movement in the selected malarial targets.

Conclusion

In order to counteract PI4KIIIβ, a new phytoconstituent derived from *B. buxifolia* roots is proposed in this work. Because of this, the existence of phytoconstituents with binding affinities for the two PI4KIIIβ targets that have been chosen is better understood via the use of computational analysis (in silico molecular docking and dynamic simulation studies). Drug development expenses, time, and adverse effects are decreased when natural compounds are investigated for potential lead molecules utilizing virtual screening techniques that make use of molecular docking analysis. It is crucial to screen ligands according to their pharmacokinetic characteristics, as this will lessen the likelihood that most medications will fail at the clinical stage. Consequently, following further investigation, 1-[2-(benzhydryloxy)ethyl]-4-(3-phenylpropyl)piperazine potentially useful natural compounds that exhibit favorable pharmacokinetic characteristics and binding energies to both 4D0L and 4WAE, may be considered as prospective malaria treatments. Better anti-malarial medications may be created by further modifying and improving these newly discovered lead chemicals. As a result, these tested compounds may provide valuable information for the creation of novel antimalarial medications.

Declarations

Author contributions PS: Formal analysis, Investigation, Methodology, Writing – original draft, Project administration and Supervision. AA: Conceptualization, Data curation, Visualization, Writing – original draft. RP; TS; and GT were involved in data collection. SK, KSR and AR: Software, Formal analysis and Methodology. All listed authors read and approved the final manuscript.

Acknowledgment

The authors would like to acknowledge the Panjab University Sophisticated Analytical Instrumentation Facility, Chandigarh, India for providing a LC-MS/HRMS facility.

Declaration of competing interest

The authors declare that they have no known competing financial interests or personal relationships that could have appeared to influence the work reported in this paper.

Funding

This research did not receive any specific grant from funding agencies in the public, commercial, or not-for-profit sectors.

Ethics approval and consent to participate: This article does not contain any studies with human participants or animals performed by any of the authors.

References

1. Adeyemo AO, Aborode AT, Bello MA et al., (2022) Malaria vaccine, the lasting solution to malaria burden in Africa. Ann med Surg 79:104031. https://doi.org/10.1016/j.amsu.2022.104031.
2. Afoakwah C, Deng X, Onur I (2018) Malaria infection among children under-five, the use of large-scale interventions in Ghana. BMC public health 18:1–13. https://doi.org/10.1186/s12889-018-5428-3.
3. World Health Organization (2022) World malaria report. Geneva, World Health Organization. https://www.who.int/teams/global-malaria-programme/reports/world-malaria-report-(2022).
4. Adia MM, Anywar G, Byamukama R et al (2014) Medicinal plants used in malaria treatment by Prometra herbalists in Uganda. J Ethnopharmacol. 155:580–588. https://doi.org/10.1016/j.jep.2014.05.060.
5. Ngarivhume T, Van't Klooster CI, De Jong JT et al (2015) Medicinal plants used by traditional healers for the treatment of malaria in the Chipinge district in Zimbabwe. J Ethnopharmacol 159:224–237. https://doi.org/10.1016/j.jep.2014.11.011.
6. Delang L, Paeshuyse J, Neyts J (2012) The role of phosphatidylinositol 4-kinases and phosphatidylinositol 4-phosphate during viral replication. Biochem Pharmacol 84:1400–1408. https://doi.org/10.1016/j.bcp.2012.07.034.
7. Dornan GL, McPhail JA, Burke JE (2016) Type III phosphatidylinositol 4 kinases, structure, function, regulation, signalling and involvement in disease. Biochem Soc Trans 9:260–266. https://doi.org/10.1042/bst20150219.
8. Paquet T, Manach CL, Cabrera DG et al (2017) Antimalarial efficacy of MMV390048, an inhibitor of Plasmodium phosphatidylinositol 4-kinase. Sci Transl Med 9 (387). https://doi.org/10.1126/scitranslmed.aad9735.
9. Taweechai S, CRISPR-Cas9 based validation of potential antimalarial targets etheses.whiterose.ac.uk (2022) Doctoral dissertation. University of Leeds
10. Doyno C, Sobiera DM, Baker WL (2020) Toxicity of chloroquine and hydroxychloroquine following therapeutic use or overdose. Clin Toxicol 59 (1) 12–23, https://doi.org/10.1080/15563650.2020.1817479.
11. Basaki M, Hashemvand A, Tayefi-Nasrabadi H et al (2022) Artemisinin and l-carnitine combination therapy alters the erythrocytes redox status. Cell Biol Int 46 (7) 1137–4. https://doi.org/10.1002/cbin.11793.
12. Ullah R, Alqahtani AS, Noman OMA et al (2020) Review on ethno-medicinal plants used in traditional medicine in the Kingdom of Saudi Arabia. Saudi J Biol Sci 27 (10) 2706–1. https://doi.org/10.1016/j.sjbs.2020.06.020.
13. Lekhak MM, Patil SS, Deshmukh PV et al (2022) Rastogi, Genus Barleria L (Acanthaceae), a review of its taxonomy, cytogenetics, phytochemistry and pharmacological potential. J Pharm Pharmacol 74:812–842. https://doi.org/10.1093/jpp/rgab183.
14. Chander PA, Sri HY, Sravanthi NB et al (2014) In vitro anthelmintic activity of Barleria buxifolia on Indian adult earthworms and estimation of total flavonoid content. Asian Pac J Trop Dis 4:S233–S235. http://dx.doi.org/10.1016/s2222-1808(14)60445-x.
15. Gopalakrishnan S, Neelakantan S, Raman PV et al (1984) Chemical examination of the roots of Barleria buxifolia Linn. Structure of barleriaquinone. Chem Pharm Bull 32:4137–4139. https://doi.org/10.1248/cpb.32.4137.
16. Ramaiah M, Gandhidasan R, Narayanan V et al (1997) ChemInform Abstract, Anthraquinone Pigments of Barleria buxifolia Linn. Chem Inform 23:39. https://doi.org/10.1002/chin.199739202.

17. Makmur T, Siregar F, Siregar S et al (2022) Open Clinical Trial of Sambiloto (Andrographis paniculata) Ethanolic Extract Capsules in Treatment of Malaria Patients in Batubara District Indonesia. Arch Med 76:419. https://doi.org/10.5455/medarh.2022.76.419-425.
18. Gopalan S, Kulanthai K, Sadashivam G et al (2016) Extraction, isolation, characterization, semi-synthesis and antiplasmodial activity of Justicia adathoda leaves. Bangladesh J Pharmacol 11:878. https://doi.org/10.3329/bjp.v11i4.28569.
19. Asante-Kwatia E, Baah MK, Forkuo AD et al (2023) Nketia, Gyimah, Lord, A.Y. Mensah, A Study on Justicia flava (Forssk.) Vahl, Pharmacognostic Characterization and Antiplasmodial and Anti-Inflammatory Properties of the Leaves. Sci World J 1–12. https://doi.org/10.1155/2023/9133288.
20. Kifle ZD, Atnafie SA (2020) Anti-Oxidant Potential and Antimalarial Effects of Acanthus polystachyus Delile (Acanthaceae) Against Plasmodium berghei, Evidence for in vivo Antimalarial Activity. J Exp Pharmacol 575–577. https://doi.org/10.2147/jep.s282407.
21. Jayapal J, Tangavelou AC, Panneerselvam A (2014) Studies on the Plant diversity of Muniandavar Sacred Groves of Thiruvaiyaru, Thanjavur, Tamil Nadu, India. Hygeia JD Med 6:48–62. https://doi.org/10.15254/h.j.d.med.6.2014.122.
22. Sivaraj N, Pandravada SR, Venkateswaran K et al (2017) Ethnic Medicinal Plant Wealth of Eastern Ghats, Status, Knowledge Systems and Conservation Strategies. Int J Curr Res Biosci Plant Biol 4:83–101. https://doi.org/10.20546/ijcrbp.2017.401.010.
23. Gangaram S, Naidoo Y, Dewir YH, El-Hendawy S (2021) Phytochemicals and Biological Activities of Barleria (Acanthaceae). Plants 11:82. https://doi.org/10.3390/plants11010082.
24. Sekar V, Balakrishnan C, Kathirvel P et al (2022) Ultra-sonication-enhanced green synthesis of silver nanoparticles using Barleria buxifolia leaf extract and their possible application. Artif Cells Nanomed Biotechnol 50:177–187. https://doi.org/10.1080/21691401.2022.2084100.
25. Jeyasankar A, Chinnamani T, Chennaiyan V et al (2014) Antifeedant activity of Barleriabuxifolia (Linn.) (Acanthaceae) against Spodoptera liturafabricius and Helicoverpaarmigerahübner (Lepidotera, Noctuidae). Int J Nat Sci Res 2:78–84. https://doi.org/10.9734/arrb/2016/23691.
26. Tamil Selvi S, Jamuna S, Thekan S et al (2017) Profiling of bioactive chemical entities in Barleria buxifolia L. using GC-MS analysis – a significant ethno medicinal plant. Journal of Ayurvedic and Herbal Medicine 3:63–77. http://dx.doi.org/10.31254/jahm.2017.3204.
27. Kapilraj PK (2016) Prophylactic and Curative Activity of 'Barleria Buxifolia. Linn' on Experimentally Induced calcium Oxalate Nephrolithiasis in Animal Model. Int J Pharmacol Clin Sci 4:68–75. https://doi.org/10.5530/ijpcs.4.4.1.
28. Johnson Inbaraj J, Krishna MC, Gandhidasan R et al (1999) Cytotoxicity, redox cycling and photodynamic action of two naturally occurring quinones1Part of this work was presented at the Second International Conference on Bioradicals and Fifth International Workshop on ESR (EPR) Imaging and in vivo ESR Spectroscopy. BBA 1472:462–470. https://doi.org/10.1016/s0304-4165(99)00150-6.
29. Patel OPS, Beteck RM, Legoabe LJ (2021) Antimalarial application of quinones: A recent update. Eur J Med Chem 210:113084. http://dx.doi.org/10.1016/j.ejmech.2020.113084.
30. Tisnerat C, Dassonville-Klimpt A, Gosselet F et al (2022) Antimalarial drug discovery, from quinine to the most recent promising clinical drug candidates. Curr Med Chem 29:3326-3365. https://doi.org/10.2174/0929867328666210803152419.
31. Bernardes LSC, Zani CL, Carvalho I (2013) Trypanosomatidae Diseases, From the Current Therapy to the Efficacious Role of Trypanothione Reductase in Drug Discovery. Curr Med Chem 20:2673–96. https://doi.org/10.2174/0929867311320210005.
32. Swamy GJ, Sangamithra A, Chandrasekar V (2014) Response surface modeling and process optimization of aqueous extraction of natural pigments from Beta vulgaris using Box–Behnken design of experiments. Dyes Pigm 111:64–74. https://doi.org/10.1016/j.dyepig.2014.05.028.
33. Wang X, Hu C, Ai Q et al (2015) Isolation and Identification Carpaine in Carica papaya, Leaf by HPLC-UV Method. Int J Food Prop 18:1505–1512. https://doi.org/10.1080/10942912.2014.900785.

34. Ruttkies C, Schymanski EL, Wolf S et al (2016) (MetFrag relaunched, incorporating strategies beyond in silico fragmentation. J Cheminformatics 8:1–16. https://doi.org/10.1186/s13321-016-0115-9.
35. Dallakyan S, Olson AJ (2014) Small-Molecule Library Screening by Docking with PyRx. Methods Mol Biol 22:243–250. http://dx.doi.org/10.1007/978-1-4939-2269-7_19.
36. Englebienne P, Moitessier N (2009) Docking Ligands into Flexible and Solvated Macromolecules, 5, Force-Field-Based Prediction of Binding Affinities of Ligands to Proteins. J Chem Inf Model 49:2564–2571. https://doi.org/10.1021/ci900251k.
37. Kondapuram SK, Sarvagalla S, Coumar MS (2021) Docking-Based Virtual Screening Using PyRx Tool, Autophagy Target Vps34 as a Case Study. Molecular Docking for Computer-Aided Drug Design 463–77. https://doi.org/10.1016/b978-0-12-822312-3.00019-9.
38. Kar S, Roy K, Leszczynski J (2022) In Silico Tools and Software to Predict ADMET of New Drug Candidates. In Silico Methods for Predicting Drug Toxicity 85–115. https://doi.org/10.1007/978-1-0716-1960-5_4.
39. Daina A, Michielin O, Zoete V (2017) SwissADME, a free web tool to evaluate pharmacokinetics, drug-likeness and medicinal chemistry friendliness of small molecules. Sci. Rep 7:1. https://doi.org/10.1038/srep42717.
40. Moon A, Khan D, Gajbhiye P, Jariya M (2017) In silico prediction of toxicity of ligands utilizing admetsar. Int J Pharm Biol Sci 8:3. https://doi.org/10.22376/ijpbs.2017.8.3.b674-677.
41. Agrawal R, Punarva HB, Heda GO et al (2023) VinaLigGen: a method to generate LigPlots and retrieval of hydrogen and hydrophobic interactions from protein-ligand complexes. J Biomol Struct Dyn 11:1–4. http://dx.doi.org/10.1080/07391102.2023.2266524
42. Karabadzhak AG, Petti LM, Barrera FN et al (2017) Two transmembrane dimers of the bovine papillomavirus E5 oncoprotein clamp the PDGF β receptor in an active dimeric conformation. Proc Natl Acad Sci 114 (35). https://doi.org/10.1073/pnas.1705622114.
43. Lee J, Cheng X, Jo S, MacKerell AD et al (2016) CHARMM-GUI Input Generator for NAMD, Gromacs, Amber, Openmm, and CHARMM/OpenMM Simulations using the CHARMM36 Additive Force Field. Biophys J 110:64. https://doi.org/10.1016/j.bpj.2015.11.3431.
44. Jo S, Lim JB, Klauda JB et al (2009) CHARMM-GUI Membrane Builder for Mixed Bilayers and Its Application to Yeast Membranes. Biophys J 97:50–58. https://doi.org/10.1016/j.bpj.2009.04.013.
45. Lu W, Su X, Klein MS, Lewis IA et al (2017) Metabolite Measurement, Pitfalls to Avoid and Practices to Follow. Annu Rev Biochem 86:277–304. https://doi.org/10.1146/annurev-biochem-061516-044952.
46. Krishnamurthy NB, Ananda AP, Nagendra Prasad HS et al (2023) HR-LCMS assisted phytochemical screening of antioxidant, antibacterial activity of Priva cordifolia (L.f) Druce plant and molecular docking approach. Results in Chemistry 5:100794. http://dx.doi.org/10.1016/j.rechem.2023.100794.
47. Abd-El-Aziz NM, Hifnawy MS, El-Ashmawy AA et al (2022) Application of Box-Behnken design for optimization of phenolics extraction from Leontodon hispidulus in relation to its antioxidant, anti-inflammatory and cytotoxic activities. Scientific Reports 12 1:8829. https://doi.org/10.1038/s41598-022-12642-2.
48. Nguyen DH, Nguyen CH, Mamitsuka H (2018) Recent advances and prospects of computational methods for metabolite identification, a review with emphasis on machine learning approaches. Briefings in Bioinformatics 20:2028–2043. http://dx.doi.org/10.1093/bib/bby066.
49. Allen F, Greiner R, Wishart D (2015) Competitive fragmentation modeling of ESI-MS/MS spectra for putative metabolite identification. Metabolomics 11:98–110. https://doi.org/10.1007/s11306-014-0676-4.
50. Moreno P, Beisken S, Harsha B et al (2015) BiNChE, A web tool and library for chemical enrichment analysis based on the ChEBI ontology. BMC Bioinformatics 16:1–7. https://doi.org/10.1186/s12859-015-0486-3.
51. Boura E, Nencka R (2015) Phosphatidylinositol 4-kinases, function, structure, and inhibition. Exp Cell Res 337:136–145. https://doi.org/10.1016/j.yexcr.2015.03.028.
52. Dela DL, Paeshuyse J, Neyts J et al (2012) The role of phosphatidylinositol 4-kinases and phosphatidylinositol 4-phosphate during viral replication. Biochem Pharmacol 84:1400–1408. https://doi.org/10.1016/j.bcp.2012.07.034.

53. Arendse LB, Wyllie S, Chibale K et al (2021) Plasmodium Kinases as Potential Drug Targets for Malaria, Challenges and Opportunities. ACS Infectious Diseases 7:518–534. https://doi.org/10.1021/acsinfecdis.0c00724.
54. Ncube NB, Govender KK, Tukulula M et al (2023) A critical analysis of the binding pocket of Plasmodium falciparum Phosphatidylinositol-4-kinase enzyme. Chemistry Select 8:e202302189. https://doi.org/10.1002/slct.202302189.
55. Wang J, Zhang CJ, Chia WN et al (2015) Haem-activated promiscuous targeting of artemisinin in Plasmodium falciparum. Nature communications 6:10111. https://doi.org/10.1038/ncomms10111.
56. Paquet T, Manach CL, Cabrera DG et al (2017) Antimalarial efficacy of MMV390048, an inhibitor of Plasmodium phosphatidylinositol 4-kinase. Science Translational Medicine 9:387. https://doi.org/10.1126/scitranslmed.aad9735.
57. Hrycyna CA, Summers RL, Lehane AM et al (2014) Quinine Dimers Are Potent Inhibitors of the Plasmodium falciparum Chloroquine Resistance Transporter and Are Active against Quinoline-Resistant P. falciparum. ACS Chem Biol 9:722–730. https://doi.org/10.1021/cb4008953.
58. Younis Y, Douelle F, Feng TS et al (2012) 3,5-Diaryl-2-aminopyridines as a novel class of orally active antimalarials demonstrating single dose cure in mice and clinical candidate potential. J Med Chem 55:3479–3487. https://doi.org/10.1021/jm3001373.
59. McCarthy JS, Donini C, Chalon S et al (2020) A Phase 1, Placebo-controlled, Randomized, Single Ascending Dose Study and a Volunteer Infection Study to Characterize the Safety, Pharmacokinetics, and Antimalarial Activity of the Plasmodium Phosphatidylinositol 4-Kinase Inhibitor MMV390048. Clin Infect Dis 71:e657–e664. https://doi.org/10.1093/cid/ciaa368.

Figures

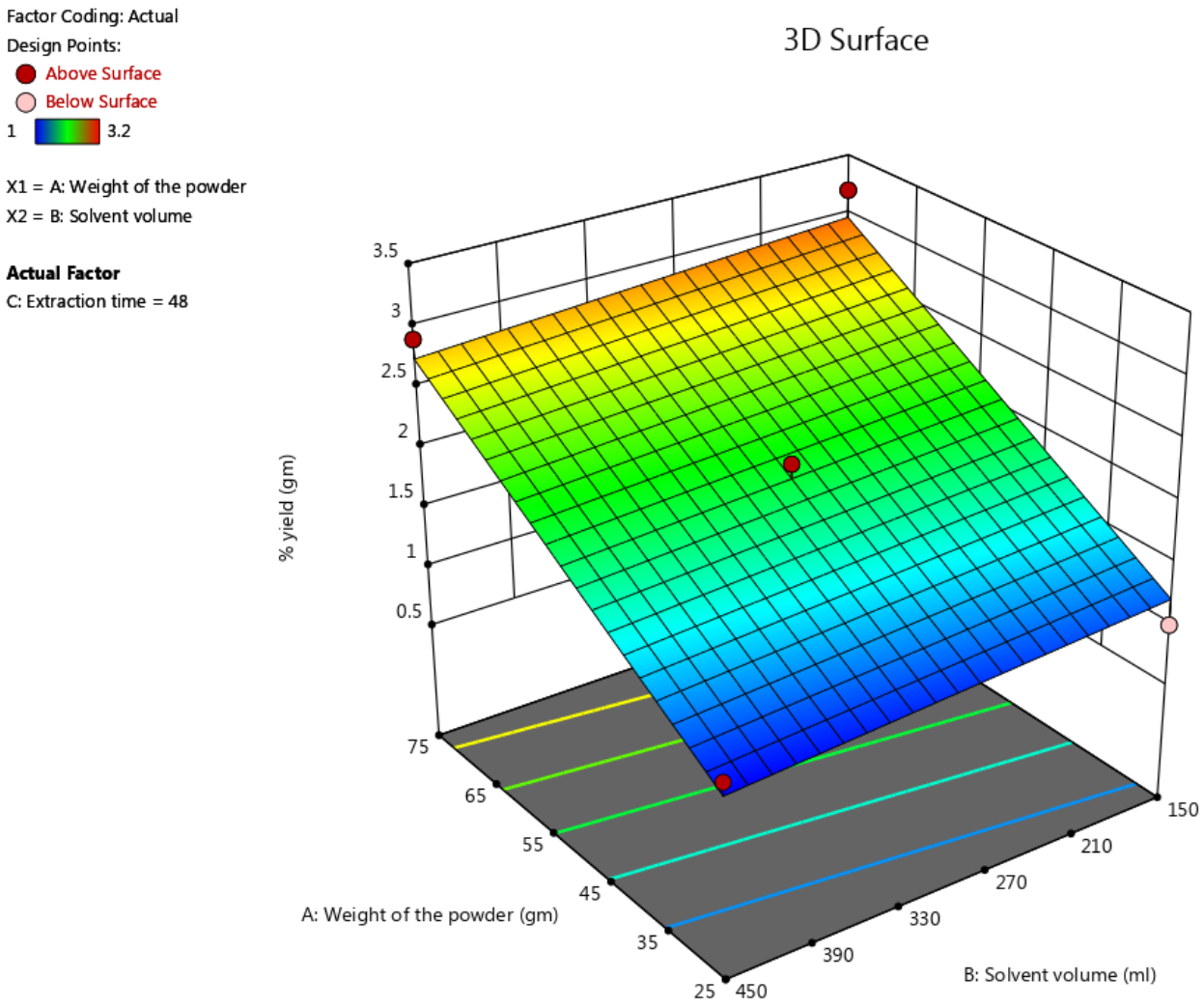

Figure 1

Response surface for the effects of solvent volume and weight of the powder on percentage yield of extraction.

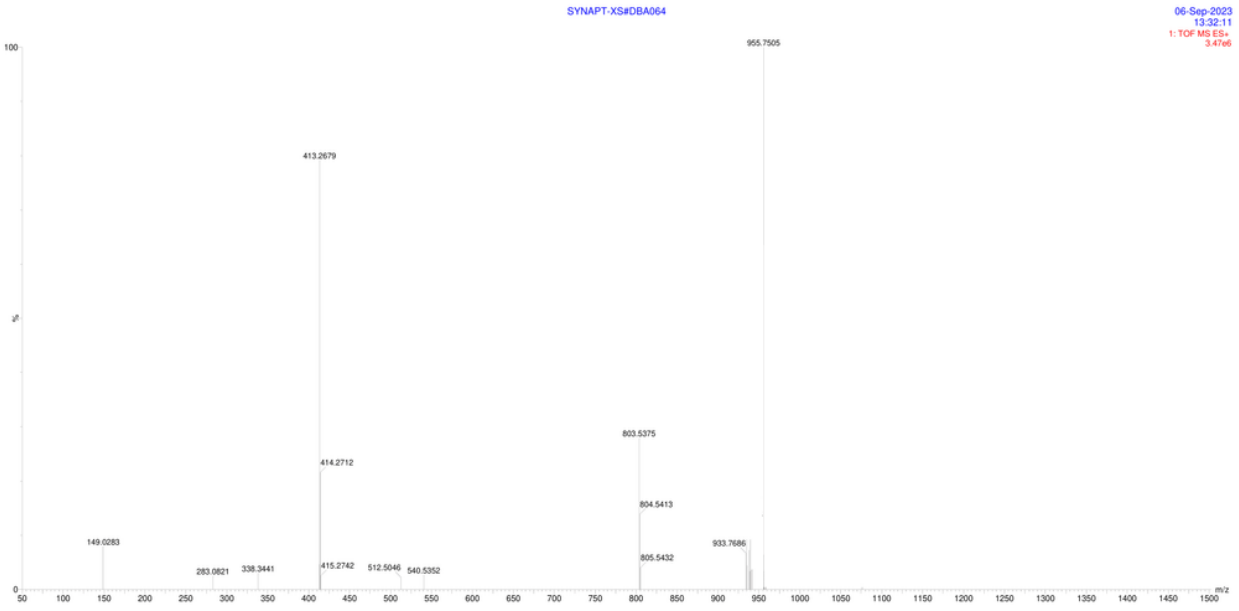

Figure 2

LC–MS/HRMS Chromatogram of extract of *B. buxifolia* root.

Fig. 3.

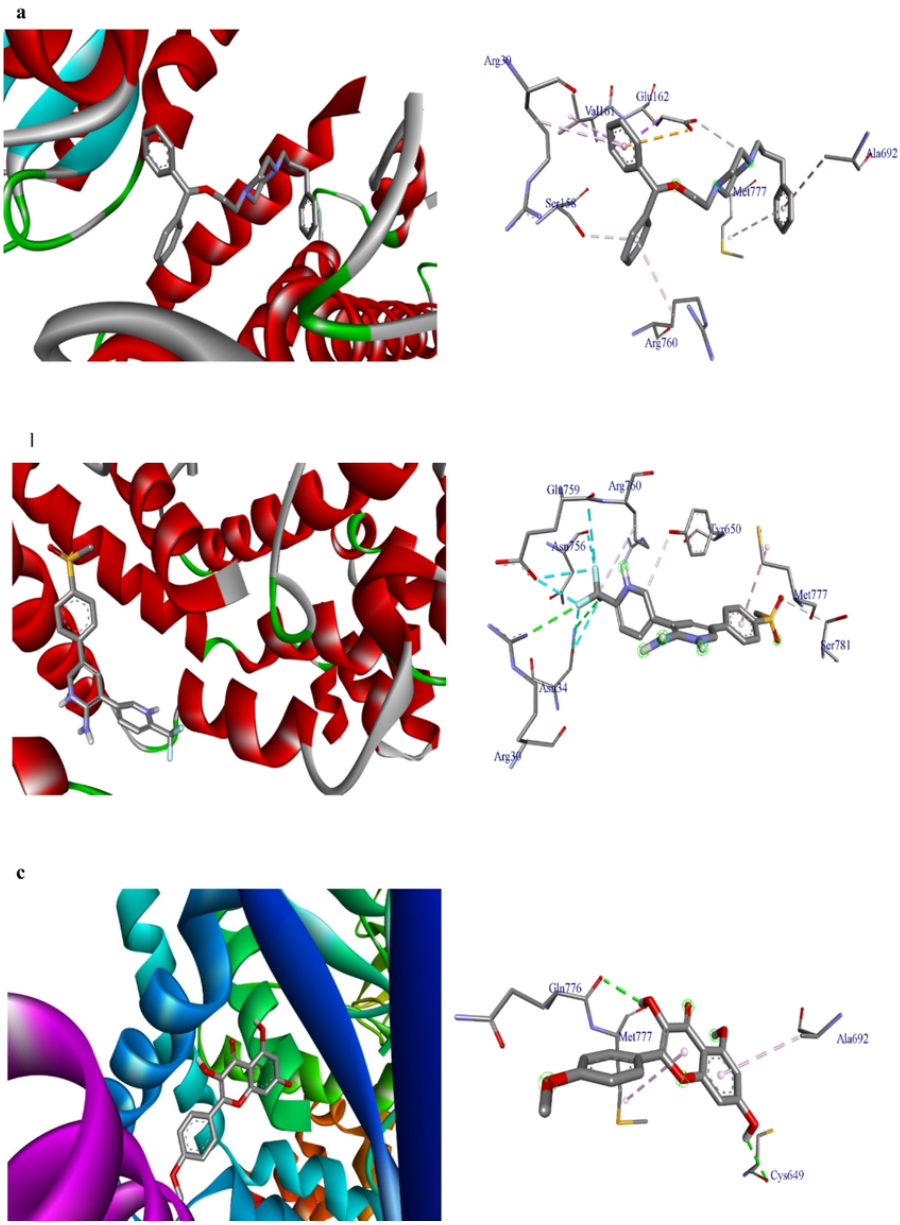

Figure 3

Docking model and binding pockets of 4D0L complex with 1-[2-(benzhydryloxy)ethyl]-4-(3-phenylpropyl)piperazine (a), MMV390048 (b) and artemisinin (c).

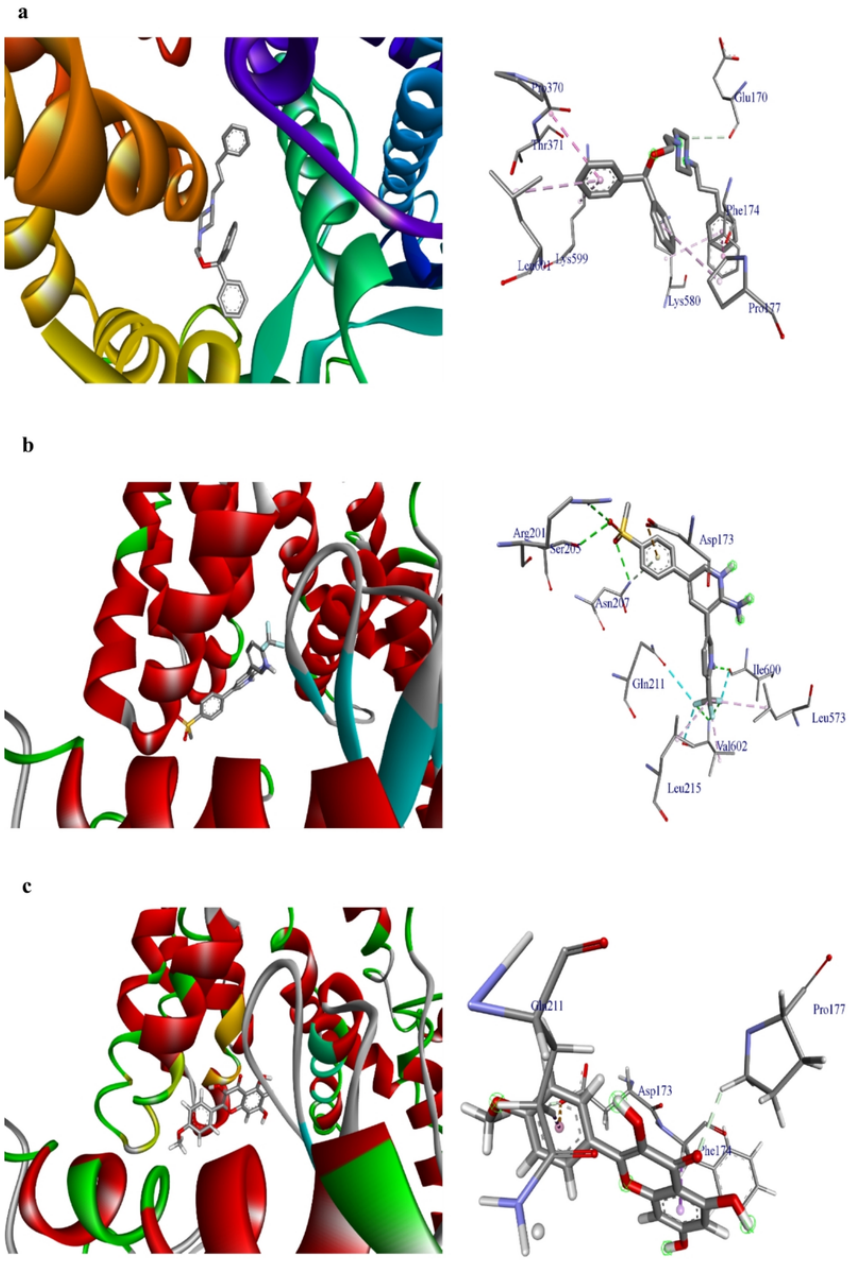

Figure 4

Docking model and binding pockets of 4WAE complex with 1-[2-(benzhydryloxy)ethyl]-4-(3-phenylpropyl)piperazine (a), MMV390048 (b) and artemisinin (c).

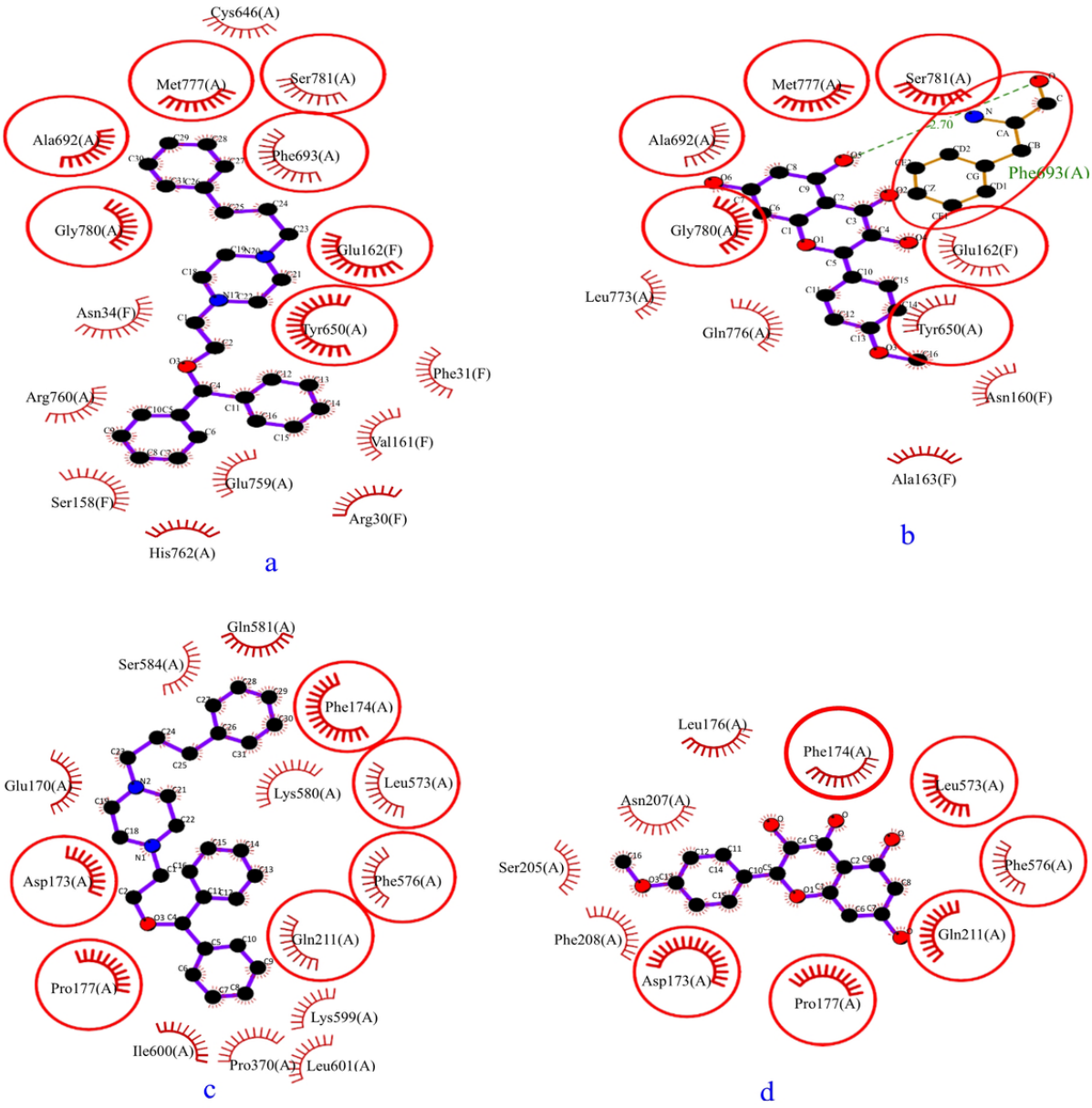

Figure 5

Ligplot analysis:4D0L with 1-[2-(benzhydryloxy)ethyl]-4-(3-phenylpropyl)piperazine (a), 4D0L with artemisinin (b), 4WAE with 1-[2-(benzhydryloxy)ethyl]-4-(3-phenylpropyl)piperazine (c), 4WAE with artemisinin (d).

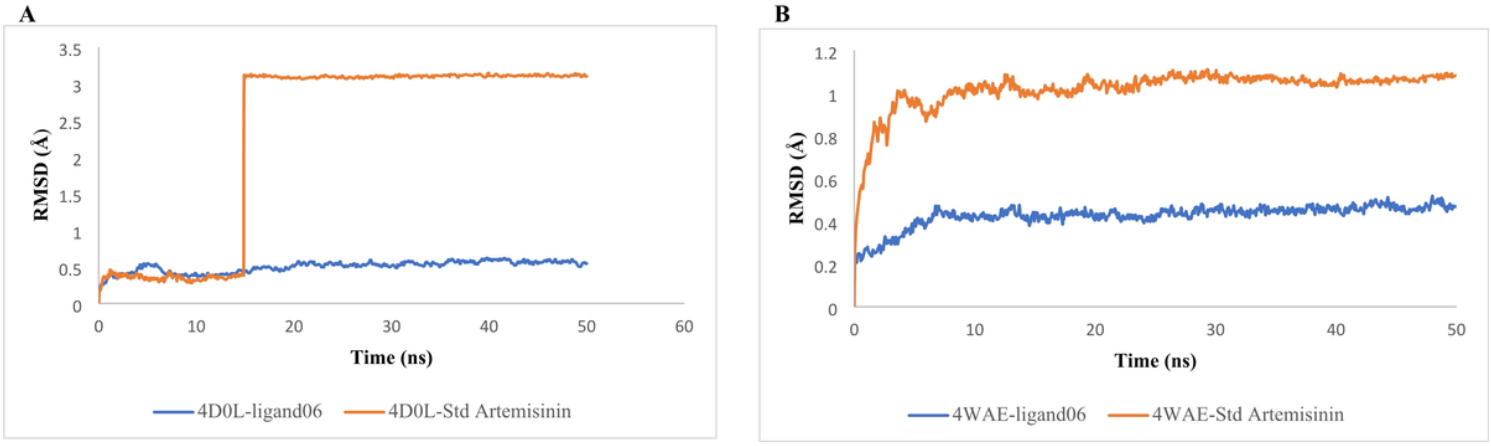

Figure 6

RMSD analysis of MD simulation trajectories: 4D0L with 1-[2-(benzhydryloxy)ethyl]-4-(3-phenylpropyl)piperazine and 4D0L with artemisinin (a); 4WAE with 1-[2-(benzhydryloxy)ethyl]-4-(3-phenylpropyl)piperazine and 4WAE with artemisinin (b).

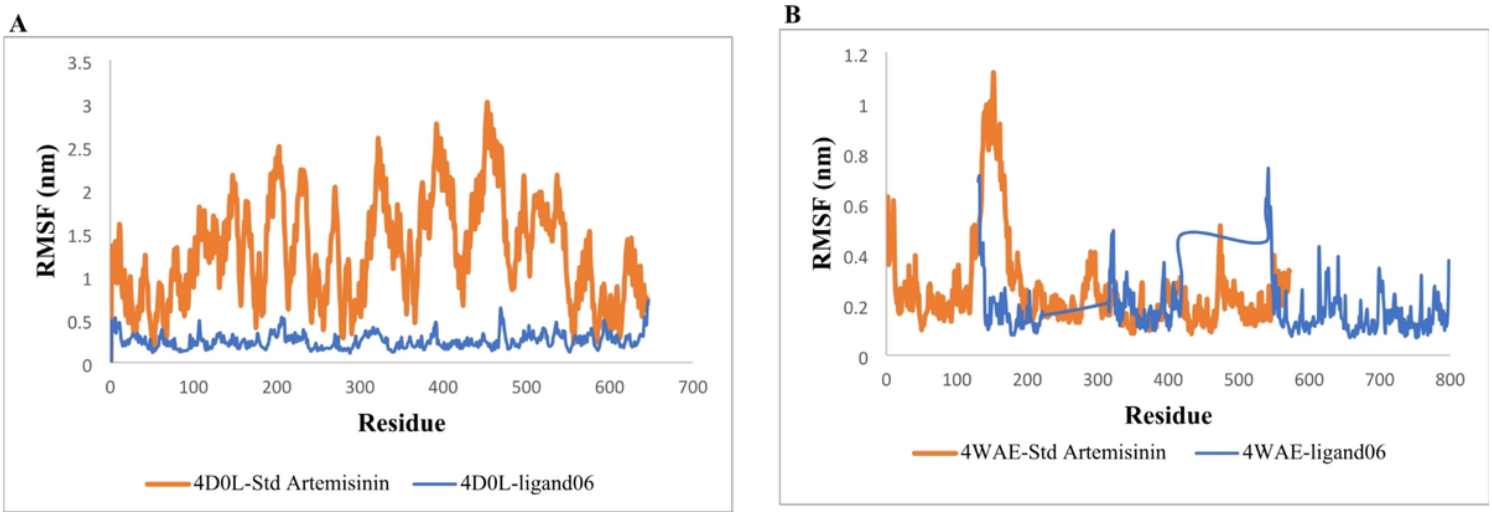

Figure 7

RMSF analysis of MD simulation trajectories: 4D0L with 1-[2-(benzhydryloxy)ethyl]-4-(3-phenylpropyl)piperazine and 4D0L with artemisinin (a); 4WAE with 1-[2-(benzhydryloxy)ethyl]-4-(3-phenylpropyl)piperazine and 4WAE with artemisinin (b).

Supplementary Files

This is a list of supplementary files associated with this preprint. Click to download.

- graphicalabstract.jpg
- SupplementaryFile.doc